# Self-energy corrections to anisotropic Fermi surfaces

R. Roldán,[1] M. P. López-Sancho,[1] F. Guinea,[1] and S.-W. Tsai[2]

[1]*Instituto de Ciencia de Materiales de Madrid, CSIC, Cantoblanco, E-28049 Madrid, Spain*
[2]*Department of Physics, University of California, Riverside, California 92521, USA*

The electron-electron interactions affect the low-energy excitations of an electronic system and induce deformations of the Fermi surface. These effects are especially important in anisotropic materials with strong correlations, such as copper-oxide superconductors or ruthenates. Here we analyze the deformations produced by electronic correlations in the Fermi surface of anisotropic two-dimensional systems, treating the regular and singular regions of the Fermi surface on the same footing. Simple analytical expressions are obtained for the corrections, based on local features of the Fermi surface. It is shown that, even for weak local interactions, the behavior of the self-energy is nontrivial, showing a momentum dependence and a self-consistent interplay with the Fermi surface topology. Results are compared to experimental observations and to other theoretical results.

PACS number(s): 71.10.Fd, 71.18.+y, 71.27.+a, 79.60.−i

## I. INTRODUCTION

Anisotropic materials present different physics at different energy scales, and their behavior or response to external probes is difficult to interpret. A large amount of experimental work hase made it possible to study the puzzling electronic properties of many anisotropic materials which, in general, present potential technological applications. More theoretical effort is needed in order to understand the detailed experimental data which reveal an unconventional behavior. In conventional metals, the excitations that govern their low-temperature physics present well-defined momenta lying at the three-dimensional Fermi surfaces. In the anisotropic materials, as layered transition metal oxides, unusual electronic properties appear and, under certain conditions, changes of the effective dimensionality occur. The electronic interaction effects are enhanced as the dimensionality decreases and can change the fundamental properties of the material.[1] Therefore, due to both the anisotropy and the periodicity along the axis perpendicular to the planes, specific collective excitations appear absent in two-dimensional (2D) and three-dimensional (3D) electron gases.[2,3]

The high-temperature cuprate superconductors are among the most studied layered transition metals oxides, treated as 2D systems in many approaches, due to its strong anisotropy. In the hole-doped cuprates the Fermi surface (FS) topology changes with doping from hole-like to electron-like.[4,5] Recently, a change in the sign of the Hall coefficient has been reported for heavily overdoped $LaSrCuO_4$.[6] The evolution of the FS in electron-doped copper-oxide superconductors with doping has been reported by angle-resolved photoemission spectroscopy (ARPES) experiments to change from electron-pocket centered at the $(\pi,0)$ point of the Brillouin zone at low doping to a hole-like FS centered at $(\pi,\pi)$ at higher doping.[7]

Other transition metal oxides as cobaltates or ruthenates are multiorbital systems and their FS present a complex topology with different sheets derived from the different bands at the Fermi energy. A correlated 2D material particularly interesting is the $Sr_2RuO_4$, a ruthenate considered a model Fermi liquid system with important electronic correlations

which have to be taken into account when interpreting photoemission spectra[8] to obtain a clear picture of the electronic properties, especially in the vicinity of the Fermi energy. In $Sr_2RuO_4$ the FS separates into three sheets $\alpha$, $\beta$, and $\gamma$, coming from the $d_{xz}$, $d_{yz}$, and $d_{xy}$ orbitals.

In the study of the electron-electron interactions in anisotropic metallic systems an open question is the deformation of the Fermi surface induced by these interactions. The Fermi surface is one of the key features needed to understand the physical properties of a material, and its shape provides important information. Recent improvements in experimental resolution have led to high precision measurements of the Fermi surface, and also to the determination of the many-body effects in the spectral function, as reported by ARPES experiments.[9] However, the interpretation of the data obtained by different experimental techniques in anisotropic strongly correlated systems remains a complex task.[10]

The Fermi surface depends on the self-energy corrections to the quasiparticle energies, which, in turn, depend on the shape of the Fermi surface. Hence, there is an interplay between the self-energy corrections and the Fermi surface topology. For weak local interactions, the leading corrections to the FS arise from second-order diagrams. The self-energy, within this approximation, can show a significant momentum dependence when the initial FS is anisotropic and lies near hot spots, where the quasiparticles are strongly scattered.[11] This simultaneous calculation of the FS and the second-order self-energy corrections is a fo rmidable task. However, the knowledge of the exact shape of the FS of a material is very important since it may affect the transport properties as well as the collective behavior, and have valuable information from the point of view of theory in order to find the appropriate model to study the system. Many approaches have been used to study this problem such as mean field,[12,13] pertubation theory,[14] bosonization methods,[15,16] or perturbative renormalization group calculations,[17–21] and the cellular dynamical mean-field theory (CDMFT), an extension of dynamical mean field theory,[22] and many others. Despite great theoretical effort done in the last years, there is a need to develop alternative new methods in order to understand the origin of the electronic properties in materials with strong correlations.

In this work, we calculate perturbative corrections and use renormalization group arguments[23,24] in order to study analytically the qualitative corrections to the shape of the FS induced by the electron-electron interaction. This method allows us to classify the different features of the FS from the dependence of the self-energy corrections on the value of the high energy cutoff $\Lambda$, defined at the beginning of the renormalization process. As will be shown later, one can also analyze the effects of variations in the Fermi velocity and the curvature of the noninteracting FS on the self-energy corrections. The calculations do not depend on the microscopic model which gives rise to a particular Fermi surface, so that it can be useful in different situations. For concreteness we will consider the $t-t'$ Hubbard model to study two-dimensional Fermi surfaces of cuprates and an extension of it to study the case of $Sr_2RuO_4$. The paper is organized as follows. We define the model in Sec. II and describe the way the self-energy corrections are calculated. In Sec. III we present a detailed calculation of the changes expected for a regular FS, as well as for a FS showing singular points like Van Hove singularities, nesting or inflexion points. We compare with results from ARPES experiments on anisotropic materials, mainly cuprate superconductors and $Sr_2RuO_4$. In the last section we highlight the most relevant aspects of our calculation, and some conclusions are presented.

## II. METHOD

The method of calculation of the self-energy corrections does not depend on the microscopic model used to obtain the electronic structure and the FS. In our scheme simple analytical expressions of the effects induced by the interactions are deduced from local features of the Fermi surface, and we are able to treat, on the same footing, the regular and singular regions of the FS. Therefore the method is particularly useful in correlated anisotropic materials which present exotic properties and deviate from band structure calculations. The importance of considering correlation effects when interpreting experimental data is already known and recently a great effort has been made in order to evaluate the self-energy from ARPES spectra.[25] The evaluation of many body effects in these complex materials is far from trivial since the electron scattering presents a dependence on momentum and energy. We limit the study to the weak coupling regime, considering weak local interactions, consistent with the Hubbard model.

### A. The model

We consider the $t-t'$ Hubbard model which is the simplest theoretical model that allows us to study different correlated materials and describes the shape of the FS observed by ARPES in different materials as cuprates (see Ref. 9 and references therein). Depending on the ratio $t'/t$ and on the band filling, different phases and stabilities appear, as found in early mean-field and quantum Monte Carlo studies of the model.[26] By changing the parameters a rich phase diagram, including antiferromagnetic, ferromagnetic and superconducting phases, has been found for the 2D $t-t'$ Hubbard model which describes many physical features of copper-

oxides and of $Sr_2RuO_4$.[27] For the cuprates, the most studied model is the Hubbard model on a square lattice and considering an effective single band. The Hamiltonian of the $t-t'$ Hubbard model is:

$$\mathcal{H} = \sum_{s;i,j} t_{ij} c_{s,i}^\dagger c_{s,j} + U \sum_i n_{i\uparrow} n_{i\downarrow}, \tag{1}$$

where $c_{s,i}(c_{s,i}^\dagger)$ are destruction (creation) operators for electrons of spin $s$ on site $i$, $n_{i,s} = c_{s,i}^\dagger c_{s,i}$ is the number operator, $U$ is the on-site repulsion, and $t_{ij} = t$ are the nearest and $t_{ij} = t'$ the next-nearest neighbors hopping amplitudes, respectively. The Fermi surfaces of the noninteracting systems are defined by

$$\epsilon_F = \varepsilon(\vec{\mathbf{k}}) = 2t[\cos(k_x a) + \cos(k_y a)] + 4t' \cos(k_x a)\cos(k_y a), \tag{2}$$

where $a$ is the lattice constant.

Assuming that $t\langle 0, t'\rangle 0$ and $|2t'| < |t|$, the Fermi surface is convex for $-2t+4t' \leqslant \epsilon_F \leqslant \epsilon_0 = -8t' + 16t'^3/t^2$. For $-8t' + 16t'^3/t^2 \leqslant \epsilon_F \leqslant -4t'$ the Fermi surface shows eight inflexion points, which begin at $k_x = k_y = k_0 = a^{-1} \cos^{-1}(-2t'/t)$ and move symmetrically around the $(\pm 1, \pm 1)$ directions, toward the center of the edges of the square Brillouin zone, $(0, \pm \pi), (\pm \pi, 0)$. For $\epsilon_F = 4t'$ the Fermi surface passes through the saddle points (Van Hove singularities) located at these special points of the Brillouin zone (BZ). For $4t' < \epsilon_F \leqslant -4t$, the Fermi surface is convex and hole-like, centered at the corners of the BZ, $(\pm \pi, \pm \pi)$. In Fig. 1 the variation of the FS shapes with doping is qualitatively shown. When only nearest-neighbor hopping is considered, $t' = 0$, the model has particle hole symmetry, and the Fermi surface shows perfect nesting for $\epsilon_F = 0$. FS shapes similar to these shown in Fig. 1 have been experimentally observed by ARPES on different cuprate samples, at different doping levels.

### B. Self-energy analysis

We will analyze the interplay between the electron-electron interactions and the FS topology in the weak-coupling regime. The corrections to the noninteracting Fermi surface are given by the real part of the self-energy. For each filling $n$, a Fermi surface is defined. The electron-electron interaction leads to a self-energy

$$\Sigma(\vec{\mathbf{k}}, \omega) = \mathrm{Re}\, \Sigma(\vec{\mathbf{k}}, \omega) + i\, \mathrm{Im}\, \Sigma(\vec{\mathbf{k}}, \omega) \tag{3}$$

which modifies the bare one-particle propagator $G_0(\vec{\mathbf{k}}, \omega)^{-1} = \omega - \epsilon_{\vec{\mathbf{k}}} + i\delta\, \mathrm{sgn}\, \epsilon_{\vec{\mathbf{k}}}$ (where $\delta \to 0^+$) to

$$G(\vec{\mathbf{k}}, \omega) = \frac{1}{\omega - [\varepsilon(\vec{\mathbf{k}}) - \epsilon_F] - \Sigma(\vec{\mathbf{k}}, \omega)} \tag{4}$$

and the FS of the interacting system is given by the $\omega = 0$ solution of the equation

$$\epsilon_F - \varepsilon(\vec{\mathbf{k}}) - \mathrm{Re}\, \Sigma(\vec{\mathbf{k}}, \omega) = 0, \tag{5}$$

where $\mathrm{Re}\, \Sigma(\vec{\mathbf{k}}, \omega)$ is the real part of the self-energy. The diagrams that renormalize the one-particle Green function up to
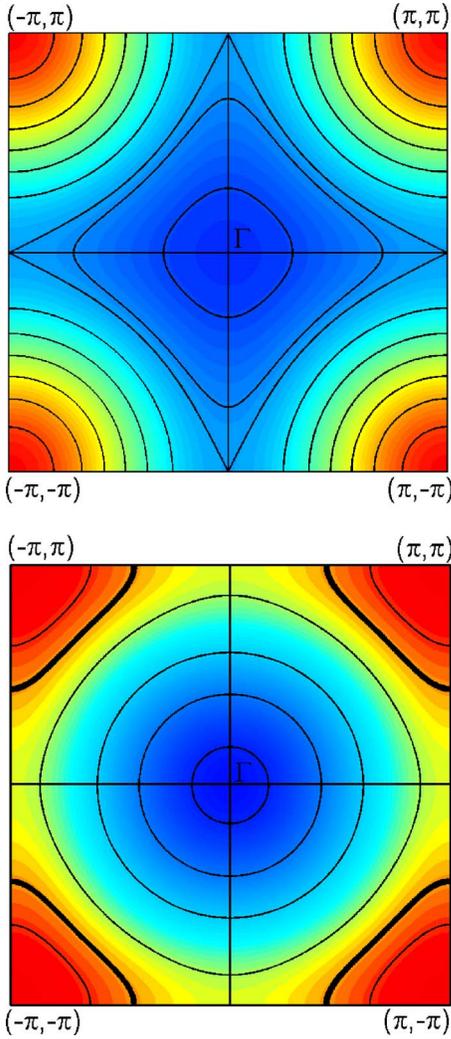
FIG. 1. (Color online) Qualitative picture of the evolution of the FS with filling from almost isotropic to convex, going through a FS exhibiting inflexion points, and one with Van Hove singularities (top panel, $t' = -0.3t$). A region with almost perfect nesting is shown in the bottom panel ($t' = 0.3t$).

second order in perturbation theory are depicted in Fig. 2 The Hartree diagram, shown at the left of the figure, gives a contribution which is independent of momentum and energy, hence it cannot deform the FS. The two-loop diagram [(b) in Fig. 2], modifies the FS through its $\vec{k}$ dependence and, in addition, it changes the quasiparticle-weight through its $\omega$ dependence.

As explained above there are many possible shapes of the FS which fit the experimental results from copper-oxide or ruthenate samples. The conventional perturbation theory fails in describing FS for which logarithmic divergences in the density of states (DOS) appear at certain values of the parameters of Eq. (1). Then we proceed to calculate the self-energy by adopting a renormalization group strategy.[23,24] It is assumed that the effect of the high energy electron-hole pairs on the quasiparticles near the Fermi surface have been integrated out, leading to a renormalization of the parameters $t, t'$ and $U$ of the Hamiltonian. The possibility that other couplings are generated in the system is not allowed. Thus,
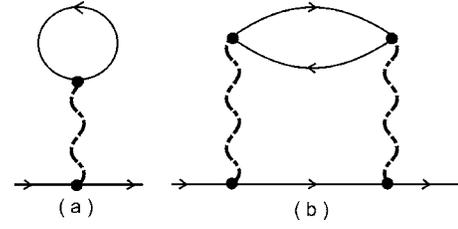


FIG. 2. Low-order self-energy diagrams. (a) Hartree diagram. (b) Two loop correction.

the Hamiltonian, Eq. (1), describes low temperature processes below a high energy cutoff, $\Lambda \ll t, t'$. For consistency, we consider the Hubbard interaction $U \lesssim \Lambda$ as well below the energy cutoff. Therefore the corrections to the quasiparticle energies are determined as a function of $\Lambda$, which defines an energy scale about the Fermi line which will contain the modes we are interested in (low energy excitations with $|\epsilon_{\vec{k}}| < \Lambda$), separated from the high energy excitations (with $|\epsilon_{\vec{k}}| > \Lambda$) which will be integrated out. We have to notice that we are restricting ourselves to a momentum-independent coupling $U$ which corresponds to a local interaction in the real space. During the process we assume that the Fermi surface of the interacting system exists, and that this FS, dressed by the corrections due to the interactions, has the same topology as that of the noninteracting system.

The two-loop self-energy shown in Fig. 2(b) can be computed from

$$i\Sigma_2(\vec{k}, \omega) = \frac{1}{(2\pi)^3} \int d\omega' \int d^2q G_0(\vec{k} - \vec{q}, \omega - \omega') \Pi(\vec{q}, \omega'),$$

(6)

where the one-loop particle-hole polarizability, in terms of the one-particle propagator, reads

$$i\Pi(\vec{q}, \omega) = \frac{U^2}{(2\pi)^3} \int d\omega' \int d^2k \Theta(\Lambda - |\epsilon_{\vec{k}}|) \Theta(\Lambda - |\epsilon_{\vec{k}+\vec{q}}|)$$

$$\times G_0(\vec{k}, \omega') G_0(\vec{k} + \vec{q}, \omega + \omega').$$

(7)

The cutoff in energies $\Lambda$ is used to implement the renormalization group (RG) scheme:[23] The virtual states in the loop of the diagram shown in Fig. 2(b) have to be kept in the energy range determined by the cutoff.

## III. RESULTS

After we compute the self-energy as explained above, we will analyze the deformation induced in the Fermi surface shape. We are interested in anisotropic two-dimensional FS similar to those measured for the cuprates which present regions with different scattering rates. For clarity, we consider first Fermi surfaces with hot spots, which are regions where the scattering of the quasiparticles is strongly enhanced. At these points, the scattering could be singular giving divergences of the susceptibility. Separately we address the deformations of regular FS, curved surfaces which do not have singularities. These surfaces present a scattering rate relatively weak. We will show that once the Fermi velocity and

curvature of the noninteracting FS are known, we can evaluate the corrections to the FS shape. Even considering a weak local interaction, without momentum dependence, the effects are strongly dependent of the location at the FS.

### A. Self-energy corrections to the Fermi surface near hot spots

In anisotropic materials, the FS can present regions or special points which are called hot spots where the quasiparticles become strongly scattered and their behavior deviates from the conventional Landau Fermi liquid. The FS of layered transition oxides, as have been shown above, change with doping adopting different shapes which lie close to Van Hove singularities, or present nested flat regions or inflexion points combined with regular sectors.

The effects of the Hubbard interaction have been studied when the Fermi surface presents hot spots both, near the perfect nesting[28–30] or near a van Hove singularity.[31–38] The curvature of the FS has important implications in the properties of the system, and the inflexion points, which separate regions where the curvature has opposite signs, may induce anomalous effects.[39,40] The crucial role that the FS geometry plays on the unusual physics of 2D systems makes desirable a deeper insight in the interplay between it and measurable parameters. The functional dependence of the self-energy on the cutoff is different in the vicinity of the hot spots than in regular zones of the FS. Near the hot spots to be considered here, the dispersion relation satisfies, near the Fermi level,

$$\epsilon_{\vec{k}} \approx \begin{cases} \pm \dfrac{k_x^2}{m_x} \mp \dfrac{k_y^2}{m_y} & \text{Van Hove,} \\ v_F k_\perp & \text{nesting,} \end{cases} \tag{8}$$

where $\epsilon_{\vec{k}} = \varepsilon(\vec{k}) - \epsilon_F$, $k_\perp$ is the momentum perpendicular to the FS relative to $k_F$, $k_\perp = (\vec{k} - \vec{k}_F)_\perp$, $v_F$ is the Fermi velocity at any particular point, and $m_x \sim m_y$.

Unlike the usual quadratic dependence expected in a Fermi liquid, the frequency dependence of the imaginary part of the self-energy in a nested region of the Fermi surface, or at Van Hove singularities is known to be linear:

$$\text{Im}\,\Sigma_2(\vec{k}, \epsilon_{\vec{k}}) \propto |\epsilon_{\vec{k}}|. \tag{9}$$

At the FS parts away from the hot spots, the leading contribution to the two-loop self-energy, when the Fermi surface is near a Van Hove singularity, comes from diagrams where the polarizability bubble, $\Pi(\vec{q}, \omega)$ expressed in Eq. (7), involves transitions near the saddle point.[41]

Only particles in the vicinity of hot spots on the FS are strongly scattered and present an anomalously large lifetime, while away from the hot spots the single particle lifetime follows Landau's Fermi liquid theory energy dependency. At some values of the band filling the FS is near a nesting situation, as shown in Fig. 1, then the polarizability at low momenta is similar to that of a one-dimensional Fermi liquid, due to the flat FS regions. The susceptibilities can be written as

$$\Pi(\vec{q}, \omega) \sim \begin{cases} W^{-1} \tilde{\Pi}_{\text{vH}} \left( \dfrac{\omega}{m^* |\vec{q}|^2} \right) & \text{Van Hove,} \\ W^{-1} \tilde{\Pi}_{\text{1D}} \left( \dfrac{\omega}{v_F |\vec{q}|} \right) & \text{nesting,} \end{cases} \tag{10}$$

where $m^*$ is an average of the second derivative of the bands at the saddle point. Note that, in both cases, the DOS is proportional to the inverse bare bandwidth $W^{-1} \sim t^{-1}, t'^{-1}$.

The imaginary part of the second-order self-energy near the regular regions of the Fermi surface can be written as[41]

$$\text{Im}\,\Sigma_2(\vec{k}, \epsilon_{\vec{k}}) \sim \int_0^{\epsilon_{\vec{k}}} d\omega \int_0^{q_{\max}} dq\, \text{Im}\,\Pi(q, \omega), \tag{11}$$

where $q_{\max} \sim |\Lambda|/v_F$, and $v_F$ is the Fermi velocity in these regions. By combining Eqs. (10) and (11), we find

$$\text{Im}\,\Sigma_2(\vec{k}, \epsilon_{\vec{k}}) \propto \begin{cases} \epsilon_{\vec{k}}^{3/2} & \text{Van Hove,} \\ \epsilon_{\vec{k}}^2 & \text{nesting.} \end{cases} \tag{12}$$

According to Eq. (12) the usual Fermi liquid result is recovered for the regular parts of the Fermi surface near almost nested regions. This result arises from the fact that the small momentum response of a quasi-one-dimensional metal does not differ qualitatively from that predicted by Landau's theory of a Fermi liquid while, close to the Van Hove singularities, the energy dependence of the $\text{Im}\,\Sigma_2(\vec{k}, \epsilon_{\vec{k}})$ presents anomalous exponents.

The effects induced by inflexion points have been addressed in Refs. 39 and 40, where the instabilities of anisotropic 2D systems are analyzed. Near the inflexion points, the dispersion relation can be expanded about the Fermi level and satisfies

$$\epsilon_{\vec{k}} \approx \begin{cases} v_F k_\parallel + b_1 k_\perp^3 & \text{inflexion point,} \\ v_F k_\parallel + b_2 k_\perp^4 & \text{special inflexion point,} \end{cases} \tag{13}$$

where $k_\parallel$ is the momentum parallel to the FS relative to $k_F$, $k_\parallel = (\vec{k} - \vec{k}_F)_\parallel$, $k_\perp$ is the momentum perpendicular to the FS relative to $k_F$, $k_\perp = (\vec{k} - \vec{k}_F)_\perp$, and $b_{1,2}$ are constants. The special inflexion points lie along a reflection symmetry axis of the BZ (Ref. 40) (the $k_x = k_y = k_0$ points). We use the techniques previously developed in Refs. 39 and 40 to obtain the second-order self-energy near an inflexion point:

$$\text{Im}\,\Sigma_2(\vec{k}, \epsilon_{\vec{k}}) \propto \epsilon_{\vec{k}}^{3/2}. \tag{14}$$

In the case of a special inflexion point, where the Fermi surface changes from convex to concave and a pair of inflexion points are generated for $\epsilon_F = \epsilon_0$ and $\vec{k} \equiv (k_0, k_0)$ defined earlier, the imaginary part of the self-energy behaves as $\text{Im}\,\Sigma_2(\vec{k}, \epsilon_{\vec{k}}) \propto \epsilon_{\vec{k}}^{5/4}$.

Once the imaginary part of the self-energy is known, we can obtain the real part of the self-energy from it by means of a Kramers-Kronig transformation. Although $\text{Im}\,\Sigma_2(\vec{k}, \epsilon_{\vec{k}})$ has been given for $\omega = \epsilon_{\vec{k}}$, since we are in the weak coupling regime $U \simeq \Lambda \ll \epsilon_F$, where $\epsilon_F$ is of the order of the noninteracting bandwidth, then the imaginary part of the self-energy associated to a state with energy $\epsilon_{\vec{k}}$ is only significant in an

energy range $-\Lambda + \epsilon_{\vec{k}} \lesssim \omega \lesssim \Lambda + \epsilon_{\vec{k}}$. We assume that one can approximate $\mathrm{Im}\,\Sigma_{\vec{k}}(\omega)$ in this range by an expansion on $(\omega - \epsilon_{\vec{k}})/W$, where $W$ is an energy scale of the order of the bandwidth in the noninteracting problem, and keep only the lowest-order term. This approximation neglects contributions from a region of energies centered around $|\omega - \epsilon_{\vec{k}}| \simeq \Lambda$ and of width $\delta\Lambda$, which is, at most, a fraction of $\Lambda$. The contribution of the Kramers-Kronig transformation performed in this region of energies is, at most, of order $\mathrm{Im}\,\Sigma_{\vec{k}}(\Lambda)$ and does not modify the dependence of $\mathrm{Re}\,\Sigma_{\vec{k}}(\epsilon_{\vec{k}})$ on the local properties of the Fermi surface. Therefore we can obtain the real part of the self-energy from the imaginary part by a Kramers-Kronig transformation, and restricting the frequency integral to the interval $0 \leq \omega \leq \Lambda$, we obtain

$$\mathrm{Re}\,\Sigma_2(\vec{k}, \epsilon_{\vec{k}}) \propto -g^2|\Lambda| \times \begin{cases} \log^2\!\left(\dfrac{\Lambda}{\epsilon_{\vec{k}}}\right) & \text{Van Hove,} \\[2ex] \log\!\left(\dfrac{\Lambda}{\epsilon_{\vec{k}}}\right) & \text{nesting,} \end{cases}$$

(15)

where the negative sign is due to the fact that it is a second-order contribution in perturbation theory, and $g$ is a dimensionless coupling constant of order $U/W$. The sign is independent of the sign of $U$ in Eq. (1). In the regular parts of the Fermi surface, Eq. (12) leads to

$$\mathrm{Re}\,\Sigma_2(\vec{k}, \epsilon_{\vec{k}}) \propto \begin{cases} -g^2\dfrac{|\Lambda|^{3/2}}{W^{1/2}} & \text{Van Hove,} \\[2ex] -g^2\dfrac{|\Lambda|^2}{W} & \text{nesting,} \end{cases}$$

(16)

where the additional powers in $W$ arise from the $m^*$ and $v_F$ factors in the susceptibility, expressed in Eq. (10).

In the limit $\Lambda/W \to 0$, the different dependence on $\Lambda$ of the self-energy corrections at different regions of the Fermi surface is enough to give a qualitative description of the changes of the Fermi surface. For instance, when the noninteracting Fermi surface is close to the saddle point, $\vec{k} \equiv a^{-1}(\pm\pi, 0), a^{-1}(0, \pm\pi)$, the self-energy correction is negative and highest in this region. Note that the logarithmic divergences in Eq. (15) are regularized by the temperature or elastic scattering.

At band fillings where the FS lies close to the Van Hove singularities, most of the low energy states close to the Fermi energy are around the saddle points $(0, \pm\pi)$ and $(\pm\pi, 0)$ (see Fig. 1). Strong screening processes arise due to the big density of states at these points, and if the chemical potential of the system is kept fixed, i.e., the system is in contact with a charge reservoir, the number of particles varies and the Fermi energy tends to be pinned at the Van Hove singularities.[42] Then, in order to remove the Fermi surface from a Van Hove point or nesting situation, a large number of electrons must be added to the regular regions. When the points of the FS near these hot spots are at distance $k$ from the hot spot, the change in the self-energy needed to shift the Fermi surface by an amount $\delta k$ is, using Eq. (15),

$$\delta\Sigma \propto g^2\Lambda\frac{\delta k}{k} \tag{17}$$

with additional logarithmic corrections near a Van Hove singularity. Near the regular regions of the Fermi surface, a shift in energy of order $\delta\Sigma$ leads to a change in the momentum normal to the Fermi surface of magnitude $\delta k_{\mathrm{reg}} \sim \delta\Sigma/v_F$. The area covered in this shift gives the number of electrons which are added to the system near the regular regions of the Fermi surface. We find

$$\delta n \sim k_{\max}\delta k_{\mathrm{reg}} \sim g^2\frac{k_{\max}\Lambda}{v_F}\frac{\delta k}{k}, \tag{18}$$

where $k_{\max} \sim a^{-1}$ determines the size of the regular regions of the Fermi surface. The value of $\delta n$ diverges as the Fermi surface moves toward the hot spot $k \to 0$. Hence, the number of electrons needed to shift the FS away from the hot spot also diverges. This result has been obtained from calculations at fixed chemical potential,[38,42] where the presence of a charge reservoir is considered, with regular self-energy corrections. This situation has particular interest when studying the physics of high-$T_c$ cuprates, where doping of the CuO$_2$ layers and interactions with the rest of the perovskite structure are important. The pinning of the Fermi level to the Van Hove singularity has been investigated in the 2D $t-t'$ Hubbard model by RG techniques,[43] taking into account the formation of flat bands due to the renormalization of the electron spectrum. The pinning of the Fermi level to the Van Hove singularities is found without making use of a reservoir, and the chemical potential of the system remains practically constant in a range of dopings near the Van Hove filling.

### B. Self-energy corrections to regular Fermi surfaces

In this section we study a 2D system at a band filling which yields a curved FS, slightly anisotropic, in the absence of singularities. Near the Fermi surface, by choosing an appropriate coordinate system, the electronic dispersion can be approximated by

$$\epsilon_{\vec{k}} = v_F k_\perp + \beta k_\parallel^2, \tag{19}$$

where $\epsilon_{\vec{k}} = \varepsilon(\vec{k}) - \epsilon_F$, $k_\perp$ is the momentum perpendicular to the FS relative to $k_F$, $k_\perp = (\vec{k} - \vec{k}_F)_\perp$, $k_\parallel$ is the momentum parallel to the FS relative to $k_F$, $k_\parallel = (\vec{k} - \vec{k}_F)_\parallel$, $v_F$ is the Fermi velocity at any particular point $v_F = \hat{\mathbf{n}}_\perp \cdot \nabla\varepsilon(\vec{k})$, and $\beta$ is related to the local curvature of the Fermi surface $b = \hat{\mathbf{n}}_\parallel \cdot [\nabla^2\varepsilon(\vec{k})]\hat{\mathbf{n}}_\parallel$, by $\beta = bv_F/2$. This expansion implies, without assuming any rotational symmetry, a FS locally indistinguishable from a circular one, where the energy Eq. (19) would correspond to a radius $k_F = m_F v_F$, where we have renamed $\beta = 1/2m_F$, $m_F$ being the effective mass. The Fermi velocity $v_F$ and the FS curvature $b$, are functions of $t, t', \epsilon_F$ and the position along the Fermi line. We calculate the second-order diagram of Fig. 2, assuming that the main contribution to the self-energy arises from processes where the momentum transfer is small, forward scattering channel, or from processes which involve scattering from the region un-

der consideration to the opposite part of the Fermi surface, i.e., backward scattering (in the Appendix we give the expressions of the polarizability for these two channels). This assumption can be justified by noting that we are considering a local Hubbard interaction, which is momentum independent, so that the leading effects are associated to the structure of the DOS. The processes discussed here are those joining the regions which have the highest DOS.

From Eq. (6) we can obtain the imaginary part of the self-energy, which describes the decay of quasiparticles in the region under consideration and that it is independent of the cutoff $\Lambda$. The contribution from forward scattering processes is

$$\text{Im}\,\Sigma_2(\vec{k},\omega) = \frac{3}{64} \frac{U^2 a^4}{\sqrt{2}\,\pi^2} \frac{\omega^2}{v_F^2 |\beta|}. \quad (20)$$

The quadratic dependence of energy is expected, and consistent with Landau's theory of a Fermi liquid. This contribution diverges as $v_F \to 0$, that is, when the Fermi surface approaches a Van Hove singularity, or as $|b| \to 0$ which signals the presence of an inflexion point or nesting. The contribution due to backward scattering is exactly the same as that from forward scattering, Eq. (20), with the same numerical prefactors.

Using a Kramers-Kronig transformation, and integrating in the interval $0 \leq \omega \leq \Lambda$, we obtain

$$\text{Re}\,\Sigma_2(\vec{k},\omega) = -\frac{3}{64} \frac{U^2 a^4}{\sqrt{2}\,\pi^3} \frac{1}{v_F^2 |\beta|}$$
$$\times \left( \Lambda^2 + 2\Lambda\omega + 2\omega^2 \log \left| \frac{\Lambda - \omega}{\omega} \right| \right). \quad (21)$$

From the experimental point of view the determination of the scattering rate $[\text{Im}\,\Sigma(\vec{k},\omega)]$ presents particular interest and much effort has been devoted in order to obtain it: by ARPES because of the momentum and energy-resolved measurements[8,25,44,45] and recently by electrical transport experiments at microwave frequencies.[46]

The extraction of the correlation functions from the experimental data is a complicated task and, although many theoretical approximations exist, the computation of correlation effects is also difficult. From ARPES results in underdoped and optimally doped cuprate samples[45] an anisotropic scattering rate around the Fermi surface has been found and the bare Fermi velocity has been directly obtained. By using a different methodology the real and imaginary parts of the self-energy has been obtained from photoemission data by a self-consistent procedure.[25]

In Fig. 3 we represent the self-energy as a function of the frequency according to results from Eqs. (20) and (21), where the linear (quadratic) behavior of the real (imaginary) part of the self-energy at low frequencies, typical of a Fermi liquid system, is recovered. We find a qualitative agreement with the low-energy part of the self-energy functions extracted self-consistently from the experiments in Refs. 25 and 47. It should be noted that we consider here the electron-electron scattering only. The impurity and electron-phonon scattering will, no doubt, cause finite lifetime and energy
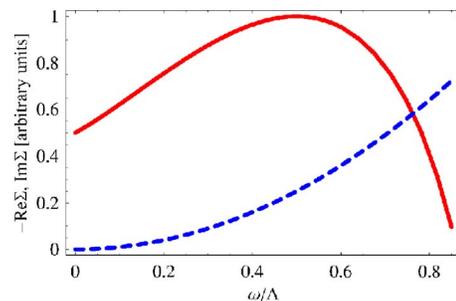


FIG. 3. (Color online) Real and imaginary parts of the self-energy as a function of the energy $\omega$: full red line $-\text{Re}\,\Sigma$, dashed blue line $\text{Im}\,\Sigma$

renormalization of the excitations but our main concern is the self-energy due to electron-electron correlation. The impurity scattering term can be considered to be isotropic (from an isotropic distribution of static impurity scatterers) an it will give a constant term in $\text{Im}\,\Sigma(\vec{k},\omega)$. The electron-phonon self-energy can be assumed to be small at low temperature. Then, the assumption that the dominant scattering mechanism is the electron-electron interaction in the systems under study is not unreasonable.[8] The essential features of the electron-phonon coupling are explained in Ref. 48, both in the superconducting and normal states. An effective $\text{Re}\,\Sigma$ is extracted from ARPES measurements and by fitting and modelling of the data information about bosonic excitations.

As a last result, from the real part of the self-energy Eq. (21), we can calculate the quasiparticle weight

$$Z_{\vec{k}_F} = \left( 1 - \frac{\partial\,\text{Re}\,\Sigma(\vec{k}_F,\omega)}{\partial\omega} \right)^{-1}_{\omega\to 0} \quad (22)$$

which for our case reads

$$Z_{\vec{k}_F} = \frac{1}{1 + \dfrac{3\sqrt{2}\,a^4}{64\pi^3} \dfrac{U^2\Lambda}{|\beta|v_F^2}}. \quad (23)$$

In the weak coupling regime, the quasiparticle weight would be minimum either if the Fermi velocity becomes very small (Van Hove singularity, consistent with results in Ref. 49) or if the curvature of the Fermi surface changes sign (inflexion point).

Finally, from Eq. (21) we obtain the expression which gives the zero frequency limit of the real part of the self-energy

$$\text{Re}\,\Sigma_2(\vec{k},\omega=0) = -\frac{3}{64} \frac{U^2 a^4}{\sqrt{2}\,\pi^3} \frac{\Lambda^2}{v_F^2 |\beta|} \quad (24)$$

which renormalizes the FS according to Eq. (5).

## C. Application to Fermi surfaces of copper-oxide superconductors

As stated in the Introduction, copper-oxide superconductors have a strongly anisotropic layered structure. Cuprates present anomalous properties in many physical aspects and
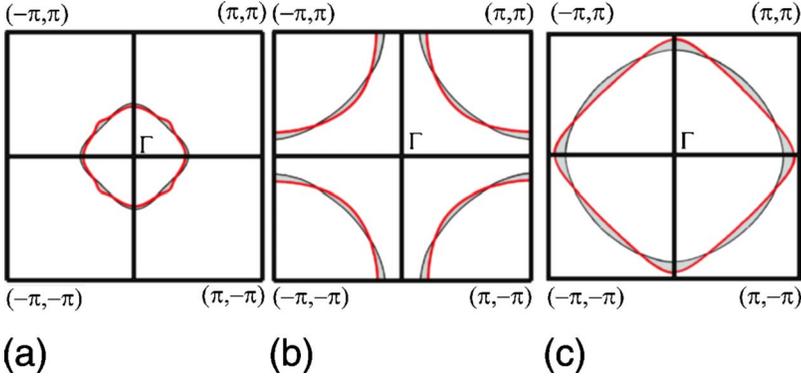
FIG. 4. (Color online) Deformations induced by the interactions on the FS of the $t-t'$ Hubbard model. The axes are labeled in units of $a^{-1}$, where $a$ is the lattice constant. The black line represents the unperturbed FS while the red (gray) line represents the FS corrected by the interaction. For $t'/t=-0.3$ (a): high doping range and (b) close to half-filling. For $t'/t=+0.3$ (c) close to half-filling.

are one of the main challenges to condensed matter physics. The peculiarities of the phase diagram have been addressed by different techniques and no consensus has been reached. Experimental results indicate a behavior far from the Fermi liquid, and the changes induced by doping on the ground state character of the normal state add complexity to the problem. Both, the low dimensionality (CuO$_2$ planes) together with the strong electronic correlations, have to be taken into account to understand the low energy excitation spectrum of the cuprates. The effects of the strong correlations on the Fermi surface shapes of the cuprates is a hot issue. Recently Civelli et al.[22] have addressed the problem by using an extension of the dynamical mean-field theory, the cellular dynamical mean-field theory (CDMFT) which allows the study of $k$-dependent properties. They study the 2D Hubbard model in the strongly correlated regime ($U=16t$). A strong renormalization of the FS shape, due to in-

teractions, is found together with a momentum space differentiation: appearance of hot and cold regions in the Brillouin zone.

We study, as well, the two-dimensional Hubbard model on a square lattice, and we will consider hopping amplitudes $t_{ij}$ to nearest neighbors $t$ and to next-nearest neighbors $t'$. Since we are in the perturbative regime we consider local weak coupling instead of the strong coupling addressed in Ref. 22. We adopt the hopping values $t=-1$ and $t'=-0.3t$ which mimic the hole-doped cuprates ($t/t'<0$), and we will consider two different doping levels. In Eq. (24) we can see how the self-energy corrections due to electron-electron interactions depend on local features of the noninteracting FS, as the Fermi velocity $v_F$ and the curvature $b$. For the dispersion relation given by Eq. (2), the expressions derived for the Fermi velocity and the curvature (taking for simplicity $a=1$) at the Fermi level, are

$$v_F(\vec{k}) = \sqrt{(t + 2t' \cos k_y)^2 \sin^2 k_x + (t + 2t' \cos k_x)^2 \sin^2 k_y},$$ (25)

$$b(\vec{k}) = -\frac{(t + 2t' \cos k_x)(t + 2t' \cos k_y)\{t \cos k_y \sin^2 k_x + 2t' \cos^2 k_y \sin^2 k_x + [t \cos k_x - t'(-3 + \cos 2k_x)]\sin^2 k_y\}}{[(t + 2t' \cos k_y)^2 \sin^2 k_x + (t + 2t' \cos k_x)^2 \sin^2 k_y]^{3/2}},$$ (26)

where $\vec{k}$ stands for the Fermi momentum $\vec{k}_F$. These expressions illustrate the momentum dependence of the self-enegy corrections. At high doping, the FS presents an almost square shape with rounded corners. We find that the self-energy corrections are stronger for the regions with the smallest curvature at the diagonal parts of the BZ. This behavior, shown in Fig. 4(a) for $\epsilon_F=-2.3\approx 8t'$, is similar to the result obtained by Freire et al. in Ref. 50 for the renormalization of a flat FS by a two-loop field theory RG approach, where interactions induce a small curvature to the bare flat FS. They found as well that the renormalized FS becomes truncated due to the interactions, not found here. Next we will consider a lower doping level. By changing the filling, the FS shape varies, and close to half-filling, for $\epsilon_F=-0.9=3t'$, the FS has the form shown in Fig. 4(b) The change in shape qualitatively agrees with the doping evolution of $k_F$ measured by ARPES on cuprates,[4,5] and the FS shape is similar to the FS reported

in different experiments. At this doping, close to half-filling, the self-energy corrections enhance the hole-like curvature around $(\pm\pi, \pm\pi)$ and $(\pm\pi, \mp\pi)$, and flatten the FS close to the $(\pm\pi,0)$ and $(0,\pm\pi)$ points of the BZ as is shown in Fig. 4(b). This result coincides with the renormalization found in Ref. 22 even though they are in the strongly correlated regime.

Corrections found in Fig. 4 can be understood by looking at Fig. 5 where the real part of the self-energy is depicted at $\omega=0$ in the square BZ. At the central region of the BZ near the $\Gamma$ point, the main corrections occur around the diagonal of the BZ, as we have found in the high doping case, where the flat parts of the noninteracting FS become curved. At this point, the larger contribution to Re $\Sigma(\vec{k}, \omega)$ will be due to the curvature of the Fermi surface, which is almost flat in the nodal region at this value of the band filling. In fact, it can be observed in Fig. 5, following the $(-\pi, -\pi)-(\pi, \pi)$ diagonal
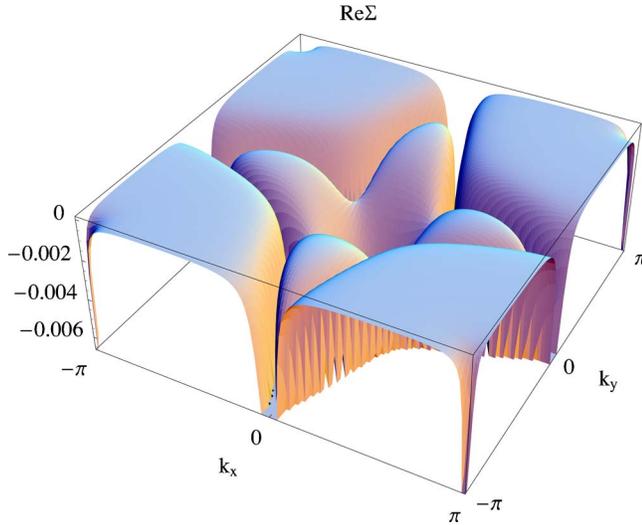
FIG. 5. (Color online) Real part of the self-energy for $t' = -0.3t$ represented in the square Brilluoin zone.

line, that the minima of $\mathrm{Re}\,\Sigma(\vec{\mathbf{k}},\omega)$ coincide with the minima of the curvature, that corresponds to the maximum correction to the noninteracting FS.

Looking again at Fig. 5 we see that, for higher fillings, the corrections are more pronounced where inflexion points start to appear in the Fermi surface (see Fig. 1). The first of these inflexion points $k_0$ occurs in the diagonal of the BZ, in the nodal direction. Once this first inflexion point appears, if we increase the occupation toward half-filling, new inflexion points merge in each FS and they distribute themselves symmetrically with respect to the diagonals of the BZ. This is why the *divergence valley* has this star-like structure. Finally, at lower doping levels, as that represented in the right panel of Fig. 4, the Fermi line reaches the region closer to the border of the BZ, and the main corrections appear at the proximity of the antinodal points $(0, \pm\pi)$, $(\pm\pi, 0)$. As can be observed in Fig. 5, $\mathrm{Re}\,\Sigma(\vec{\mathbf{k}}, 0)$ shows pronounced dips close to the saddle points, and therefore the FS is renormalized in this region. These minima are due to Van Hove singularities where the $v_F$ vanishes.

This result agrees with one-loop functional RG calculation of the self-energy in the weak coupling regime of the 2D $t-t'$-Hubbard model at Van Hove band fillings[49] where vanishing of the quasiparticle weight on approaching the antinodal points is found. Away from the Van Hove fillings a quasiparticle peak, with small spectral weight, emerges at $(\pi, 0)$ and $(0, \pi)$.

The case of an electron-doped system can be analyzed by a particle-hole transformation of the Hamiltonian which re-

verses the sign of $t'$, $(t/t' > 0)$. For $t' = +0.3t$ we find that, close to half-filling, the self-energy corrections are stronger in the proximity of the saddle points, where $v_F \rightarrow 0$. As can be seen in Fig. 4(c), the corrected FS is closer to a nesting situation than the bare FS.
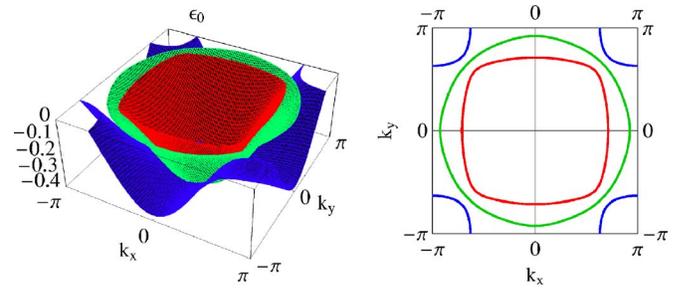
Our results, near half-filling, are in overall agreement with those of Ref. 22, although we find that the self-energy corrections are stronger at the antinodal region in both, hole-like and electron-like, Fermi surfaces.

### D. Application to Fermi surface of Sr$_2$RuO$_4$

Sr$_2$RuO$_4$ is a highly anisotropic layered compound, with an electrical anisotropy of about 4000.[51] It has a strongly two-dimensional electronic structure and exhibits a good Fermi liquid behavior below 30 K, as probed by bulk transport measurements.[51] The Fermi surface measured by ARPES matches the de Haas van Alphen measurements and it can be well described by band structure calculations. Therefore Sr$_2$RuO$_4$ is considered a correlated 2D material. As it occurs in the cuprates, the competition between superconducting and magnetic instabilities plays an important role in the low energy physics of Sr$_2$RuO$_4$ which, with a critical temperature of about $T_c \approx 1.5$ K, presents an unconventional superconductivity with a $p$-wave and spin-triplet pairing.[52] This material has three relevant bands,[53] $\alpha$, $\beta$, and $\gamma$, of $t_{2g}$ symmetry, formed from the $4d$ orbitals of the Ru$^{4+}$ ion. The $\{\alpha, \beta\}$ bands are derived from $\{d_{xz}, d_{yz}\}$ orbitals and form two quasi-one-dimensional bands along the directions $z$ and $y$, respectively, that are weakly hybridized. The $\gamma$ band is derived from the $d_{xy}$-orbital and disperses into a real 2D band. In Fig. 6 are depicted the electronic structure, left panel and corresponding FS, right panel, calculated following the dispersion relation



FIG. 6. (Color online) Left: Band structure of Sr$_2$RuO$_4$ obtained from Eq. (27) using the parameter values given in Ref. 54. The blue (outer) sheet corresponds to the $\alpha$ band, the red (inner) sheet is the $\beta$ band, and the green sheet corresponds to the $\gamma$ band. Right: Corresponding Fermi surface.

$$\varepsilon_\gamma(\vec{\mathbf{k}}) = -2t_{1\gamma}[\cos(k_x a) + \cos(k_y a)] - 4t_{2\gamma}\cos(k_x a)\cos(k_y a) - \varepsilon_{0\gamma},$$

$$\varepsilon_{\alpha,\beta}(\vec{\mathbf{k}}) = -(t_{1\alpha,\beta} + t_{2\alpha,\beta})[\cos(k_x a) + \cos(k_y a)] \pm \sqrt{\{(t_{1\alpha,\beta} - t_{2\alpha,\beta})[\cos(k_x a) - \cos(k_y a)]\}^2 + 16t_{3\alpha,\beta}^2 \sin(k_x a)^2 \sin(k_y a)^2} - \varepsilon_{0\alpha,\beta}.$$

$$(27)$$
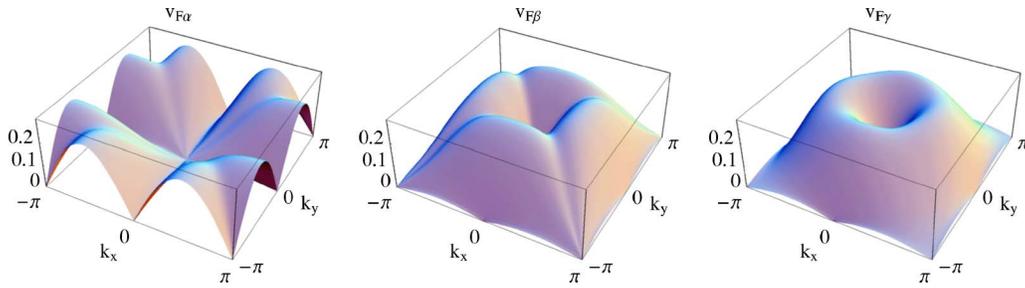
FIG. 7. (Color online) Fermi velocity of the noninteracting bands: The left graph corresponds to the $\alpha$ band, center graph corresponds to $\beta$ band, and right graph corresponds to $\gamma$ band of $Sr_2RuO_4$.

The tight-binding parameters are taken from Ref. 53 and 54 This FS is in good agreement with that reported by ARPES experiments and obtained by band calculations. As before, the self-energy corrections to the three sheets of the FS depend on the Fermi velocity and the curvature (not given here due to its size). In Fig. 7 we can see the momentum dependence of the Fermi velocity for the three bands. It is easy to appreciate that the minima of the three plots are, besides in the $\Gamma$ point, in the antinodal points, $(\pm\pi, 0)$ and $(0, \pm\pi)$, and in the diagonal of the BZ, $(\pm\pi, \pm\pi)$ and $(\pm\pi, \mp n)$.

The momentum dependence of the real part of the self-energy for the three bands is shown in Fig. 8. In the left-hand side we can see the correction to the $\alpha$ sheet, that is significant only either when the Fermi line lies near the $\Gamma$ point or in the proximity of the corners of the BZ, $(\pm\pi, \pm\pi)$ points. In a recent experimental work,[8] the form of $Im\Sigma(\omega)$ extracted for the bulk $\alpha$ band from the ARPES spectra is found to be consistent with a Fermi liquid, and that the quasiparticles residing in the surface layer $\alpha$ band show similar many-body interactions. (Notice that the analysis and fitting procedure over raw data of this band made in Ref. 8 leads to self-energy curves of the form of Fig. 3). In the central figure, the contribution corresponding to the $\beta$ band is shown. Here we can see that the correction is maximum (most negative) in the zones between the diagonals, due to the nearly flat regions of the Fermi line corresponding to the $\beta$ band.

Finally, the corrections to the $\gamma$ band are shown in the right-hand side of Fig. 8 (notice the different scales in the three graphs). In this case the corrections are maxima near the antinodal points $(\pm\pi, 0)$ and $(0, \pm\pi)$, due to the proximity of this band to a Van Hove point. In Ref. 54 it is pointed

out that calculated $\gamma$ band properties depend very sensitively on how close it approaches the Van Hove points $(\pi, 0)$, $(0, \pi)$.

The main corrections occur at the $\gamma$ band, as is shown in Fig. 9 where the bare and renormalized FS are depicted. Here noninteracting FS (full blue line) is changed, due to electron-electron correlations, to the interacting FS (dashed red line). This result agrees with photoemission measurements which indicate that the $\gamma$-band has much stronger interactions and plays a dominant role at low temperature.[55]

The corrections in the $\alpha$ and $\beta$ bands are due to curvature effects, while the corrections to the $\gamma$ band are due to Fermi velocity effects, because of the proximity of this band to the saddle points, as has been pointed out above. Then, in agreement with ARPES measurements[8] and other theoretical results,[54] the main corrections induced in the FS of $Sr_2RuO_4$ occur at the $\gamma$-band corresponding sheet. The importance of the FS geometry has been analyzed in Ref. 54 where the nonanalytic corrections to the specific heat and susceptibility of a 2D Fermi liquid have been considered and the results applied to $Sr_2RuO_4$. Both, the dependence of the $\gamma$ band properties on how close the band approaches the Van Hove points and the dominant interaction in the $\gamma$ band are found in Ref. 54, because it has the highest density of states at the Fermi level, as well as the largest mass and susceptibility enhancements.[53]

Similarly, the importance of the band structure properties of these materials can be seen in the context of multilayer ruthenates, for which the proximity of their Fermi surface to a Van Hove singularity can give rise to a quantum critical end point in the magnetic phase diagram, as it is found, within a mean-field analysis, in Ref. 56.
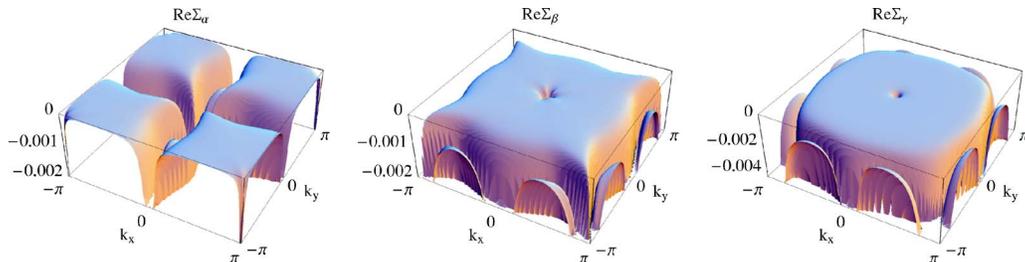


FIG. 8. (Color online) Real part of the self-energy corrections for the three bands of $Sr_2RuO_4$ in the first square BZ: The left graph corresponds to the $\alpha$ band, middle graph to the $\beta$ band, and right graph corresponds to $\gamma$ band. We have used the parameter values $U$ =0.01 and $\Lambda$=1. Notice the different scales in the three graphs.
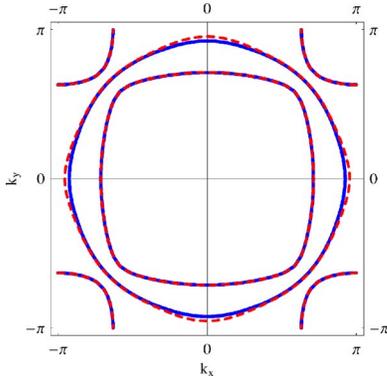
FIG. 9. (Color online) Bare (continuous blue) and interacting (dashed red) Fermi surface of $Sr_2RuO_4$.

## IV. CONCLUSIONS

The unconventional physics shown by anisotropic materials, as high-$T_c$ superconductors and ruthenates, poses big difficulties when a theoretical model has to be chosen. On the other hand, although it is generally accepted that the many-body interactions of electrons play a key role in the underlying physics of these compounds and may be related to the occurrence of superconductivity in the cuprates, a consensus has not been reached about the origin of important features widely observed by different experimental techniques. The anisotropy momentum space shown by many electronic properties of the planes adds complexity to the possible theories.

In the cuprates, the pseudogap phase, metallic but with a broken Fermi surface (segments known as Fermi arcs[57]) is an example of the remarkable momentum dependence of the interactions. Furthermore, the band renormalization observed by ARPES in different families of high-$T_c$ superconductors, known as kink in the dispersion, which indicates a strong coupling to a collective mode (see Ref. 48 and references therein), shows different energy scales and temperature dependence at the nodal and antinodal regions of the BZ, suggesting two different kinks of different origin, whose nature is under debate: both phonon and magnetic mode have been suggested as possible causes.

More recently, a high energy anomaly in the spectral function has been observed in three different families of high-$T_c$ superconductors, and apparently in several ruthenate compounds.[58] This anomaly indicates that the quasiparticles at $\epsilon_F$ are dressed not only by the interactions with bosons at low energy, but also by interactions at higher energies. This peculiar high energy behavior together with the unconventional low energy properties, poses a challenge on theoretical models.

The knowledge of the dressed FS is crucial to understand the behavior of correlated materials, especially when an effective model is needed to explain the unconventional physics. We have presented here a simplified way of taking into account the self-energy corrections to the Fermi surface. We have made use of the different dependence of the self-energy on the high energy cutoff in order to analyze the main features of the changes of the FS. The analysis presented here is valid only at weak coupling, and we do not consider correc-

tions to the interactions or to the wave-function renormalization. On the other hand, the expressions obtained are analytical and related to the local features of the noninteracting FS in a simple way, so that they can be readily used to get an estimate of the corrections expected.

The results suggest that the main self-energy corrections, which are always negative in our scheme, peak when the FS is close to the $(\pm\pi,0)$, $(0\pm\pi)$ points in the Brillouin zone. If these contributions are cast as corrections to the hopping elements of the initial Hamiltonian, we find that the nearest neighbor hopping $t$ is weakly changed (as it does not contribute to the band dispersion in these regions). The next-nearest neighbor hopping $t'$, which shifts the bands by $-4t'$ in this region, acquires a negative correction. This implies that the absolute value of $t'$ grows when $t'>0$, or decreases, when $t'<0$, in reasonable agreement with the results reported in Ref. 22. Note that the tendency observed in our calculation toward the formation of flat regions near these points, when analyzed in higher-order perturbation theory, will lead to stronger corrections. Our results also confirm the pinning of the FS near saddle points, due to the interactions. The analysis presented here is consistent with the measured Fermi surfaces of the cuprates[9] and qualitatively agrees with the doping evolution reported by ARPES.[4,5,9] The self-energy corrections found for the FS of $Sr_2RuO_4$, which mainly renormalize the $\gamma$ sheet, are as well in qualitative agreement with ARPES measurements[8] and previous calculations.[54] The broad spectrum of experimental data available at this moment makes comparison between results from different techniques one of the most efficient methods to obtain information about response and correlation functions of unconventional materials. To get an estimation of the self-energy corrections to the Fermi surface in a simple way, independent of the model, as the one here proposed, is helpful in order to gain insight into many low-energy physics aspects.

## APPENDIX: POLARIZABILITY

In this appendix the particle-hole polarizability for the forward and backward scattering channels are given. These polarizabilities are calculated in oreder to obtain the self-energy Eq. (20). The imaginary part of $\Pi(\vec{q},\omega)$ for the forward channel is, using Eq. (7) and the parametrization from Eq. (19),

$$\text{Im } \Pi^F(\vec{q},\omega) = -\frac{U^2}{16\pi} \frac{|\omega|}{\beta v_F} \sqrt{\frac{2\beta}{\omega - M_{\vec{q}}^F}}, \qquad (A1)$$

where $\vec{q}$ is a small vector that connects two pieces close together in the FS and $M_{\vec{q}}^F = v_F q_\perp + \frac{2}{9}\beta q_\parallel^2$. The argument of the square root has to be positive, which gives an extra condition, $\omega\,\text{sgn}(\beta) > M_{\vec{q}}^F \text{sign}(\beta)$.

Similarly, for the backward scattering we obtain

$$\mathrm{Im}\,\Pi^{\mathrm{B}}(\vec{Q}+\vec{q},\omega) = -\frac{U^2}{16\pi}\frac{1}{\beta v_{\mathrm{F}}}\begin{cases} \sqrt{2\beta(|\omega|+\mathrm{M}^{\mathrm{B}}_{\vec{q}})}-\sqrt{2\beta(\mathrm{M}^{\mathrm{B}}_{\vec{q}}-|\omega|)} & \text{if } |\omega| < \mathrm{M}^{\mathrm{B}}_{\vec{q}}\,\mathrm{sgn}(\beta), \\ \mathrm{sgn}(\beta)\sqrt{2\beta(|\omega|\mathrm{sgn}(\beta)+\mathrm{M}^{\mathrm{B}}_{\vec{q}})} & \text{if } |\omega| > |M^{B}_{\vec{q}}|, \end{cases} \tag{A2}$$

where $\vec{q}$ is the deviation of teh wave-vector from the vector $\vec{Q}$ that connects the region studied with the opposite part of the FS, and $\mathrm{M}^{\mathrm{B}}_{\vec{q}} = \mathrm{V}_{\mathrm{F}}\mathrm{q}_{\perp} - \frac{2}{9}\beta\mathrm{q}^2_{\parallel}$.

For $\vec{q}=0$ we have that $\mathrm{Im}\,\Pi^{\mathrm{B}}(\vec{Q}+\vec{q},\omega) \sim \sqrt{|\omega|}$, which agrees with the results obtained in Ref. 59, where a spin-fluctuation model for the $Q=2k_F$ instability is studied. For small $\omega$ and fixed $\vec{q}$ we have, expanding Eq. (A2) up to first order in $|\omega|/\mathrm{M}^{\mathrm{B}}_{\vec{q}}$ [for the case $|\omega| < \mathrm{M}^{\mathrm{B}}_{\vec{q}}\mathrm{sgn}(\beta)$], that $\mathrm{Im}\,\Pi^{\mathrm{B}}(\vec{Q}+\vec{q},\omega) \sim |\omega|$, as expected for a Fermi liquid.[59]

[1] T. Valla, P. D. Johnson, Z. Yusof, B. Wells, Q. Li, S. M. Loureiro, R. J. Cavas, M. Mikami, Y. Mori, M. Yoshimura *et al.*, Nature (London) **417**, 627 (2002).

[2] E. Arrigoni, Phys. Rev. B **61**, 7909 (2000).

[3] S. Biermann, A. Georges, A. Lichtenstein, and T. Giamarchi, Phys. Rev. Lett. **87**, 276405 (2001).

[4] T. Yoshida, X. J. Zhou, K. Tanaka, W. L. Yang, Z. Hussain, Z. X. Shen, A. Fujimori, S. Komiya, Y. Ando, H. Esaki *et al.*, cond-mat/0510608 (2005).

[5] A. Kaminski, S. Rosenkranz, H. M. Fretwell, M. R. Norman, M. Randeria, J. C. Campuzano, J.-M. Park, Z. Z. Li, and H. Raffy, Phys. Rev. B **73**, 174511 (2006); cond-mat/0507106.

[6] I. Tsukada and S. Ono, cond-mat/0605720 (2006).

[7] N. P. Armitage, F. Ronning, D. H. Lu, A. Damascelli, K. M. Shen, D. L. Feng, H. Eisaki, Z. X. Shen, P. K. Mang, N. Kanebo *et al.*, Phys. Rev. Lett. **88**, 257001 (2002).

[8] N. J. C. Ingle, K. M. Shen, F. Baumberger, W. Meevasan, D. H. Lu, Z. X. Shen, A. Damascelli, S. Nakatsuji, Z. Q. Mao, Y. Maeno *et al.*, Phys. Rev. B **72**, 205114 (2005).

[9] A. Damascelli, Z. Hussain, and Z.-X. Shen, Rev. Mod. Phys. **75**, 473 (2003).

[10] S. Zhou, M. Gao, H. Ding, P. A. Lee, and Z. Wang, Phys. Rev. Lett. **94**, 206401 (2005).

[11] R. Roldán, M. López-Sancho, F. Guinea, and S.-W. Tsai, Europhys. Lett. **76**, 1(2006).

[12] B. Valenzuela and M. A. H. Vozmediano, Phys. Rev. B **63**, 153103 (2001).

[13] C. M. Varma, Philos. Mag. **85**, 1657 (2005).

[14] A. Virosztek and J. Ruvalds, Phys. Rev. B **42**, 4064 (1990).

[15] A. H. C. Neto and E. Fradkin, Phys. Rev. B **49**, 10877 (1994).

[16] J. Fjaerestad, A. Sudbo, and A. Luther, Phys. Rev. B **60**, 13361 (1999).

[17] B. Altshuler, L. Ioffe, and A. Millis, Phys. Rev. B **52**, 5563 (1995).

[18] A. Neumayr and W. Metzner, Phys. Rev. B **67**, 035112 (2003).

[19] S. Ledowski and P. Kopietz, J. Phys.: Condens. Matter **15**, 4779 (2003).

[20] H. Freire, E. Corrêa, and A. Ferraz, Phys. Rev. B **71**, 165113 (2005).

[21] S. Dusuel and B. Douçot, Phys. Rev. B **67**, 205111 (2003).

[22] M. Civelli, M. Capone, S. Kancharla, O. Pacollet, and G. Kotliar, Phys. Rev. Lett. **95**, 106402 (2005).

[23] R. Shankar, Rev. Mod. Phys. **66**, 129 (1994).

[24] W. Metzner, C. Castellani, and C. di Castro, Adv. Phys. **47**, 3 (1998).

[25] A. A. Kordyuk, S. V. Borishenko, A. Koitzsch, J. Fink, M. Knupfer, and H. Berger, Phys. Rev. B **71**, 214513 (2005).

[26] H. Q. Lin and J. E. Hirsch, Phys. Rev. B **35**, 3359 (1987).

[27] A. A. Katanin and A. P. Kampf, Phys. Rev. B **68**, 195101 (2003).

[28] A. T. Zheleznyak, V. M. Yakovenko, and I. E. Dzyaloshinskii, Phys. Rev. B **55**, 3200 (1997).

[29] F. V. Abreu and B. Doucot, Europhys. Lett. **38**, 533 (1997).

[30] A. Ferraz, Europhys. Lett. **61**, 228 (2003); Phys. Rev. B **68**, 075115 (2003); H. Freire, E. Corrêa, and A. Ferraz, cond-mat/0304347.

[31] J. Labbé and J. Bok, Europhys. Lett. **3**, 1225 (1987).

[32] J. Friedel, J. Phys. (France) **48**, 1787 (1987).

[33] J. E. Dzyaloshinskii, Pis'ma Zh. Eksp. Teor. Fiz. **46**, 118 (1987) [JETP Lett. **46**, 118 (1987)].

[34] H. J. Schulz, Europhys. Lett. **4**, 609 (1987).

[35] F. Lederer, G. Montambaux, and D. Poilblanc, J. Phys. (France) **48**, 1613 (1987).

[36] R. S. Markiewicz and B. G. Giessen, Physica C **160**, 497 (1989).

[37] D. M. Newns, H. R. Krishnamurthy, P. C. Pattnaik, C. C. Tsuei, and C. L. Kane, Phys. Rev. Lett. **69**, 1264 (1992).

[38] J. González, F. Guinea, and M. A. H. Vozmediano, Europhys. Lett. **34**, 711 (1996).

[39] J. González, F. Guinea, and M. A. H. Vozmediano, Phys. Rev. Lett. **79**, 3514 (1997).

[40] S. Fratini and F. Guinea, Phys. Rev. B **66**, 125104 (2002).

[41] R. Hlubina and T. M. Rice, Phys. Rev. B **51**, 9253 (1995).

[42] J. González, Phys. Rev. B **63**, 045114 (2001).

[43] V. Y. Irkhin, A. A. Katanin, and M. I. Katsnelson, Phys. Rev. Lett. **89**, 076401 (2002) (the pinning found in this reference depends on the existence of an almost flat dispersion relation near the saddle point).

[44] T. Valla, A. V. Fedorov, P. D. Johnson, Q. Li, G. D. Gu, and N. Koshizuka, Phys. Rev. Lett. **85**, 828 (2000).

[45] A. Kaminski, H. M. Fretwell, M. R. Norman, M. Randeria, R. Rosenkrans, U. Chatterjee, J. C. Campuzano, J. Mesot, T. Sato,

T. Takahashi *et al.*, Phys. Rev. B **71**, 014517 (2005).

[46] S. Ozcan, P. J. Turner, J. R. Waldra, R. J. Drost, P. H. Kes, and D. M. Broun, Phys. Rev. B **73**, 064506 (2006).

[47] B. P. Xie, K. Yang, D. W. Shen, J. F. Zhao, H. W. Ou, J. Wei, S. Y. Gu, M. Arita, S. Qiao, H. Namantame *et al.*, cond-mat/0607450 (2006).

[48] X. J. Zhou, T. Cuk, T. Devereaux, N. Nagaosa, and Z.-X. Shen, *Treatise of High Temperature Superconductivity*, edited by J. Robert Schrieffer (2006), cond-mat/0604284.

[49] A. A. Katanin and A. P. Kampf, Phys. Rev. Lett. **93**, 106406 (2004).

[50] H. Freire, E. Corrêa, and A. Ferraz, Physica C **408–410**, 254 (2004).

[51] A. P. Mackenzie and Y. Maeno, Rev. Mod. Phys. **75**, 657 (2003).

[52] T. M. Rice and M. Sigrist, J. Phys.: Condens. Matter **7**, L643 (1995).

[53] C. Bergeman, A. P. Mackenzie, S. R. Julian, D. Forsyte, and E. Ohmicho, Adv. Phys. **52**, 639 (2003).

[54] A. V. Chubukov and A. J. Millis, cond-mat/0604496 (2006).

[55] T. E. Kidd, T. Valla, A. V. Fedorov, P. D. Johnson, R. J. Cava, and M. K. Haas, Phys. Rev. Lett. **94**, 107003 (2005).

[56] B. Binz and M. Sigrist, Europhys. Lett. **65**, 816 (2004).

[57] A. Kanigel, M. R. Norman, M. Randeria, U. Chatterjee, S. Suoma, A. Kaminski, H. M. Fretwell, S. Rosenkranz, M. Shi, T. Sato *et al.*, Nat. Phys. **2**, 447 (2006).

[58] J. Graf, G.-H. Gweon, K. McElroy, S. Y. Zhou, C. Jozwiak, E. Rotenberg, A. Bill, T. Sasagawa, H. Eisaki, S. Uchida *et al.*, cond-mat/0607319 (2006).

[59] P. Krotkov and A. V. Chubukov, Phys. Rev. Lett. **96**, 107002 (2006).